





Arrhythmia-associated calmodulin variants interact with KCNQ1 to confer aberrant membrane trafficking and function

Po wei Kang ^a, Lucy Woodbury^a, Paweorn Angsutararux^a, Namit Sambare^a, Jingyi Shi^a, Martina Marras ^a, Carlota Abella^a, Anish Bedi^a, DeShawn Zinn^a, Jianmin Cui ^a and Jonathan R. Silva ^{a,*}

^aDepartment of Biomedical Engineering, Washington University in St. Louis, St. Louis, MO 63130, USA

*To whom correspondence should be addressed: Email: jonsilva@wustl.edu

Edited By: Josh Wand

Abstract

Missense variants in calmodulin (CaM) predispose patients to arrhythmias associated with high mortality rates (“calmodulinopathy”). As CaM regulates many key cardiac ion channels, an understanding of disease mechanism associated with CaM variant arrhythmias requires elucidating individual CaM variant effects on distinct channels. One key CaM regulatory target is the KCNQ1 (K_v7.1) voltage-gated potassium channel that carries the I_{Ks} current. Yet, relatively little is known as to how CaM variants interact with KCNQ1 or affect its function. Here, we take a multipronged approach employing a live-cell fluorescence resonance energy transfer binding assay, fluorescence trafficking assay, and functional electrophysiology to characterize >10 arrhythmia-associated CaM variants for effect on KCNQ1 CaM binding, membrane trafficking, and channel function. We identify one variant (G114W) that exhibits severely weakened binding to KCNQ1 but find that most other CaM variants interact with similar binding affinity to KCNQ1 when compared with CaM wild-type over physiological Ca²⁺ ranges. We further identify several CaM variants that affect KCNQ1 and I_{Ks} membrane trafficking and/or baseline current activation kinetics, thereby delineating KCNQ1 dysfunction in calmodulinopathy. Lastly, we identify CaM variants with no effect on KCNQ1 function. This study provides extensive functional data that reveal how CaM variants contribute to creating a proarrhythmic substrate by causing abnormal KCNQ1 membrane trafficking and current conduction. We find that CaM variant regulation of KCNQ1 is not uniform with effects varying from benign to significant loss of function, suggesting how CaM variants predispose patients to arrhythmia via the dysregulation of multiple cardiac ion channels.

Classification: Biological, Health, and Medical Sciences, Physiology

Keywords: KCNQ1, K_v7.1, calmodulin, calmodulinopathy, ion channels, arrhythmia

Significance Statement

Patients carrying mutations or variants in the protein calmodulin (CaM) are known to suffer from arrhythmias with high mortality rates. The mechanism underlying CaM-associated arrhythmias is complex because CaM modulates several ion channels in the heart. Specifically, it is largely unknown whether CaM-associated arrhythmias may be caused by dysfunction of the voltage-gated potassium channel encoded by KCNQ1. Here, we utilize fluorescence and electrophysiology techniques to determine how >10 CaM variants might change KCNQ1 binding, membrane expression, and function. Our results reveal that CaM variant effects on KCNQ1 range from minimal functional impact to significant loss of function. Altogether, these findings demonstrate that KCNQ1 dysfunction is likely to play a role in CaM-associated arrhythmia.

Introduction

Calmodulin (CaM) is a ubiquitous auxiliary subunit of key ion channels underlying the cardiac action potential. In the heart, CaM regulatory targets include ryanodine receptors (RyR2) and several voltage-gated channels including calcium channels (e.g. Ca_v1.2), sodium channels (e.g. Na_v1.5), and potassium channels (e.g. KCNQ1 or K_v7.1) (1–6). CaM canonically acts as a Ca²⁺ sensor

and confers Ca²⁺ sensitivity to channels to allow Ca²⁺-dependent inactivation in Ca_v1.2 and Na_v1.4 (1, 3, 7). Independent of Ca²⁺-sensing function, CaM binding also modulates baseline channel function in Ca_v1.2, Na_v1.5, and K_v7.1 (8–11). Inherited or de novo mutations in these channels causing CaM dysregulation are associated with arrhythmias such as Timothy syndrome (TS), Brugada syndrome (BrS), and long QT syndrome (LQTS) (9, 12–14). Three

Competing Interest: Jingyi Shi and Jianmin Cui are cofounders of a startup company VivoCor LLC, which is targeting I_{Ks} for the treatment of cardiac arrhythmia.

Received: March 20, 2023. **Accepted:** October 4, 2023

© The Author(s) 2023. Published by Oxford University Press on behalf of National Academy of Sciences. This is an Open Access article distributed under the terms of the Creative Commons Attribution-NonCommercial-NoDerivs licence (<https://creativecommons.org/licenses/by-nc-nd/4.0/>), which permits non-commercial reproduction and distribution of the work, in any medium, provided the original work is not altered or transformed in any way, and that the work is properly cited. For commercial re-use, please contact journals.permissions@oup.com

genes in the human genome (*CALM1-3*) encode for CaM with 100% conservation in amino acid identity (3, 15), and CaM was long-thought to be intolerant of primary sequence alterations. Recently, human missense variants in CaM have emerged as a molecular factor underlying arrhythmias (“calmodulinopathy”) such as LQTS and catecholaminergic polymorphic ventricular tachycardia (CPVT) that are associated with high mortality rates (14, 16–20). As CaM variants cause dysfunction in many combinations of their regulatory targets, calmodulinopathy mechanisms are fundamentally complex. Several studies have established that CaM missense variants impair Ca^{2+} binding (16, 21–28). To date, CaM variant effects have been evaluated for their effect on $\text{Ca}_v1.2$ or RyR2, with many shown to induce $\text{Ca}_v1.2$ and RyR2 dysfunction, thereby contributing to arrhythmogenesis (14, 22, 27, 29–34). By comparison, relatively little is known regarding whether CaM variants may also alter KCNQ1 channel function and membrane expression, with only a few studies suggesting potential effects (10, 28, 35). Moreover, the relative contributions of trafficking, gating effects, and binding are not well-delineated for different variants. These knowledge gaps represent a missing piece for in-depth understanding of calmodulinopathy mechanisms that integrate distinct CaM regulatory targets.

In the heart, KCNQ1 is a homo-tetrameric potassium channel that associates with the auxiliary subunits KCNE1 and CaM to conduct the slow delayed rectifier current (I_{Ks}), which participates in action potential repolarization primarily in the context of β -adrenergic stimulation (5, 6, 36–38). Structurally, CaM interacts with helix A (HA) and helix B (HB) within the KCNQ1 carboxy-terminus domain (CTD) as well as the S2-S3 linker within the KCNQ1 voltage-sensing domain (VSD) (Fig. 1A and B) (5, 6, 10, 35, 38, 39). CaM association with KCNQ1 is required for channel assembly and membrane trafficking (5, 6). CaM further exerts functional effects by triggering current enhancement upon elevated intracellular Ca^{2+} and modulating KCNQ1 and I_{Ks} baseline current under resting Ca^{2+} conditions (10, 39–41). KCNQ1 features a gating mechanism leveraged by CaM and KCNE1 to modulate the channel. Upon membrane depolarization, the KCNQ1 VSD activates in a two-step manner, from the resting state to a stable intermediate state and then to the activated state (38, 42–44). VSD occupancy of the intermediate and the activated states both trigger KCNQ1 pore opening, yielding two open states (42–44). KCNE1 suppresses intermediate state conductance to help delay current activation kinetics (43, 44). CaM controls channel occupancy of the activated state to modulate KCNQ1 current activation kinetics (10). Taken together, CaM missense variants have the potential to alter multiple KCNQ1 parameters from trafficking to current conductance, all of which may lead to abnormal action potential repolarization.

Here, we perform extensive characterization of 14 CaM variants to determine whether KCNQ1 dysfunction contributes to calmodulinopathy-related arrhythmias (Fig. 1B and C). The CaM variants investigated here cover nearly all currently known variant positions. We developed a fluorescence resonance energy transfer (FRET) assay to quantify CaM variants binding to full-length KCNQ1 in live cells, thereby identifying CaM variants capable of competing with CaM wild-type (WT) for binding KCNQ1. Using fluorescence assays and functional electrophysiology, we further identify specific CaM variants that confer abnormal KCNQ1 membrane trafficking or aberrant current conduction. Together, our results systematically map distinct CaM variant effects to KCNQ1 binding, membrane trafficking, and current conduction, delineating how KCNQ1 dysfunction contributes to calmodulinopathy.

Results

A FRET-based assay to probe CaM interaction with full-length KCNQ1

Although CaM is encoded by three genes in the human genome, the presence of one gene carrying a missense variant is sufficient to induce arrhythmia (16–19). This genetic pattern suggests that CaM variants and CaM WT are both expressed in cardiomyocytes. Thus, CaM variants compete with CaM WT for binding to their regulatory targets. As KCNQ1 channel assembly and membrane expression require CaM association (5, 6), the ability of CaM variants to bind to KCNQ1 critically determines whether the variant may impart current dysfunction on membrane-expressing KCNQ1. To explore this question, we developed a FRET assay to quantify binding between CaM and KCNQ1 channels in live cells. FRET is a phenomenon in which nanometer proximity ($< \sim 100 \text{ \AA}$) between two appropriate fluorophores can be optically detected and has been successfully employed to study CaM–channel interaction (29, 45–48). Here, we innovated on prior techniques through the design of a novel FRET pair between CaM and full-length KCNQ1, as well as the development of an electron multiplying charge-coupled device (EMCCD) camera-based imaging technique and automated analysis to efficiently quantify binding between CaM variants and KCNQ1 (see [Extended Methods](#)).

In developing the FRET assay, we first selected the well-characterized Cerulean–Venus FRET pair (49) and screened for optimal fluorophore placement to detect FRET signal between CaM and the full-length KCNQ1. Cerulean was labeled to the CaM carboxy-terminus by fusion, enabling the Cerulean-tagged CaM to act as a FRET donor (Fig. 1D). For the FRET acceptor, we screened for optimal labeling position by fusing a Venus to the carboxy-terminus or the cytosolic helix A–helix B (HAB) linker of the full-length KCNQ1. Insertion of a Venus fluorophore within the KCNQ1 HAB linker after residue S484, which we term KCNQ1-VenHAB, yielded a channel with grossly preserved channel trafficking and ionic conductance when assayed by two-electrode voltage-clamp (TEVC) in *Xenopus* oocytes (Fig. 1D, Fig. S1A and B). The KCNQ1 HAB linker is an ~ 100 -residue-long disordered cytosolic loop situated between the two main CaM binding helices in the KCNQ1 CTD (35, 38, 39). Previous studies have found that HAB linker truncation does not affect KCNQ1 function (50). The lack of an apparent functional role for the HAB linker may explain the channel’s tolerance to a fluorophore insertion within the HAB linker. Moreover, Cerulean-tagged CaM exhibited higher maximum FRET efficiency with KCNQ1-VenHAB ($E_{\text{Max}} \sim 0.34$) when compared with labeling Venus at the KCNQ1 carboxy-terminus ($E_{\text{Max}} \sim 0.17$) (Figs. S1 and S2). This enhanced maximum FRET efficiency is likely due to the closer distance between CaM and the KCNQ1 HAB linker as compared with the KCNQ1 carboxy-terminus, although an orientation-dependent factor cannot be ruled out. We selected KCNQ1-VenHAB as the FRET acceptor in our assay owing to its enhanced maximum FRET efficiency.

To examine binding between CaM and the full-length KCNQ1 channel, we cotransfected Cerulean-tagged CaM and KCNQ1-VenHAB in Chinese hamster ovary (CHO) cells followed by fluorescence imaging using a custom FRET microscope with an EMCCD camera and an optical splitter to simultaneously image fluorescence intensity at the donor and acceptor emission wavelengths (Fig. 1E; see [Extended Methods](#)). The acquired images were then analyzed with MATLAB software to compute an apparent FRET efficiency metric E_D in 1,580 cells across 7 independent transfections (Fig. 1E and F; also see [Extended Methods](#)). The measured

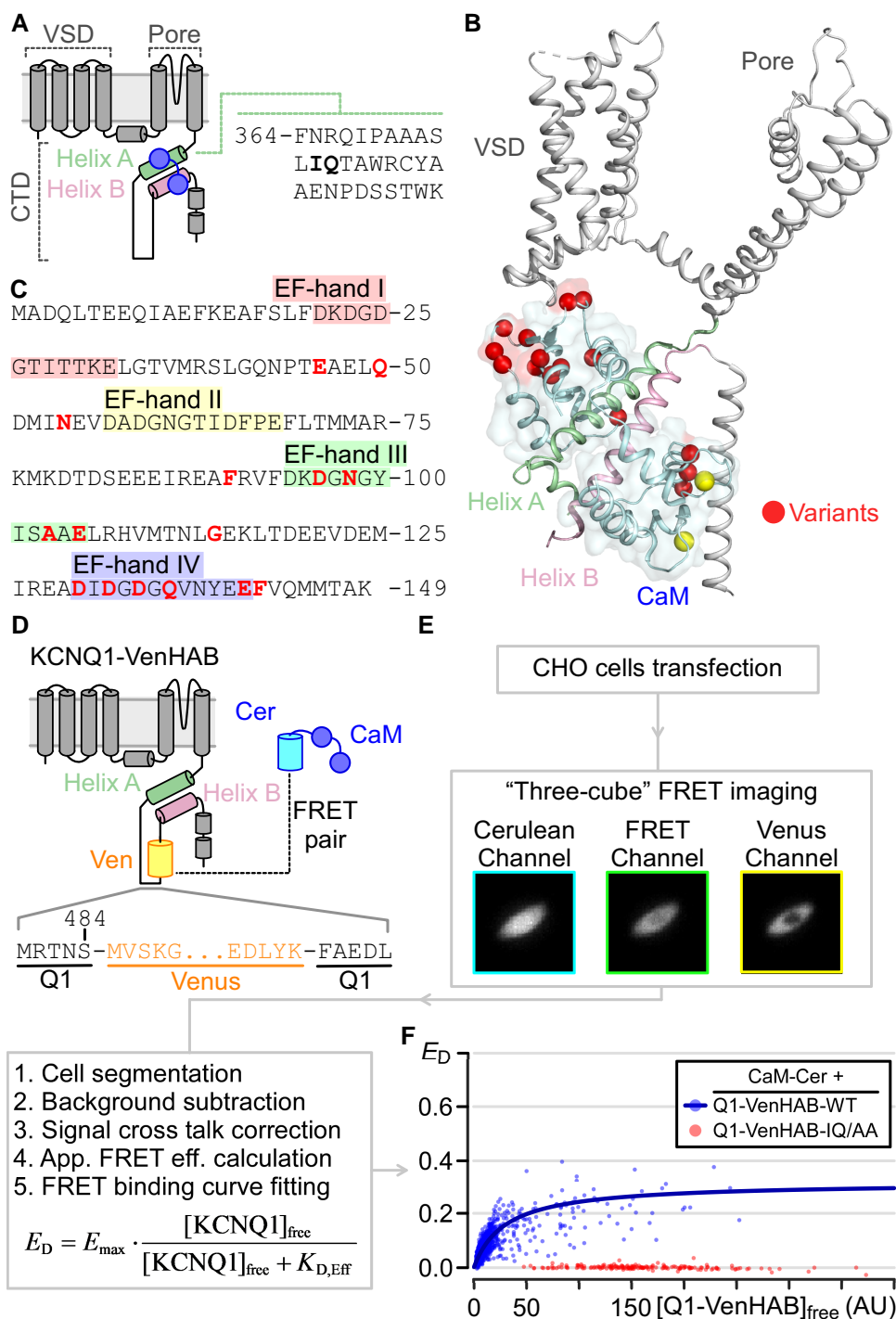


Fig. 1. A FRET-based live-cell assay to probe CaM interaction with full-length KCNQ1. A) KCNQ1 topology and CaM interacting regions. CaM binds HA and HB within the C-terminus domain (CTD) of KCNQ1. VSD is voltage-sensing domain. The sequence for KCNQ1 HA is shown, with the key CaM-interacting "IQ" residues bolded. B) Cryo-EM structural depiction (PDB: 6UZZ) of the human KCNQ1-CaM complex with red spheres indicating positions with known CaM variants. Two yellow spheres on the right side of the CaM structure are calcium ions. C) Sequence of CaM. Each EF hand (colored highlights) can coordinate one Ca^{2+} ion. Red residues correspond to positions with known CaM variants. D) Cartoon illustration of the KCNQ1-VenHAB and CaM-Cerulean FRET pair. The Venus insertion site is shown. E) FRET workflow to detect CaM interaction with full-length KCNQ1 in live cells. F) Fitted FRET binding curves of Cerulean-tagged CaM with KCNQ1-VenHAB-WT (blue [top trace], $n = 1768$) and KCNQ1-VenHAB-IQ/AA (red [bottom], $n = 217$). Each dot is one cell. For WT, best-fit $E_{\max} = 0.317$ and $K_{D,\text{eff}} = 30.2$ AU with 95% CI = (23.9, 36.7). For IQ/AA, no fitting was performed because of the lack of rise in FRET signal.

apparent FRET efficiency E_D observed in each cell depends on two main factors: (i) the true FRET efficiency influenced by the relative orientation and distance between donor and acceptor fluorophores in the bound complex (KCNQ1/CaM in this case) and (ii) the binding reaction between the protein pair (KCNQ1 and CaM) that depends on

the relative concentrations of the protein pair expressed within the cell (i.e. whether the FRET pairs are bound). Prior studies have shown that the latter factor can be leveraged to quantify relative binding affinity between the labeled FRET pairs. Specifically, variation in transfection efficiency leads to varying titration of free concentrations of

FRET donor and acceptor in each cell, enabling fitting of a FRET binding curve by imposing an appropriate binding model (47, 51, 52). The KCNQ1/CaM complex exists in a 4:4 stoichiometry (35, 38). We fitted the E_D readouts to a 1:1 (equivalent to 4:4) binding model to derive a FRET binding curve with an apparent dissociation constant ($K_{D,eff}$) related to the binding affinity between CaM and KCNQ1 (Fig. 1F; also see [Extended Methods](#)). This analysis assumed CaM and KCNQ1 binds identically and independently in a 4:4 fashion. We note it is possible that CaM binding to KCNQ1 may exhibit cooperativity, which was not modeled in the fitting process to estimate $K_{D,eff}$. We favored a 1:1 binding scheme for two reasons. First, it has not been shown that CaM interaction with KCNQ1 exhibits cooperativity. Notably, proximity between CaM and KCNQ1 tetramer does not necessitate cooperative binding. For example, cAMP has been shown to bind identically and independently to HCN channels in a 4:4 stoichiometry despite proximity (53). Second, modeling cooperativity would introduce an unconstrained free parameter in the fitting process, as the degree of cooperativity is unknown. This increases the risk of overfitting. We therefore favored a 1:1 binding scheme to constrain $K_{D,eff}$ as the only free parameter for the most robust estimation. This analysis yielded a FRET binding curve demonstrating a clear rise in E_D as the number of free KCNQ1-VenHAB increased with an estimated $K_{D,eff} = 30.2$ AU (Fig. 1F, blue dots and curve), indicating proximity and binding between Cerulean-tagged CaM and KCNQ1-VenHAB. We note that the estimated $K_{D,eff}$ is in arbitrary units (AU) but can be compared across different constructs for relative binding changes. Although our assay does not report an absolute binding affinity, our method enables quantification of CaM interaction with the full-length KCNQ1 channel within live CHO cells. Furthermore, CaM has been shown to interact with other KCNQ1 regions such as the transmembrane voltage-sensing domain (10, 35, 38), which can be difficult to reconstitute in vitro systems but is fully accounted for in our FRET assay.

To further validate our assay, we measured FRET between Cerulean-tagged CaM and KCNQ1-VenHAB carrying mutations known to disrupt CaM binding to the channel. We mutated the key “IQ” residues in KCNQ1 HA (Fig. 1A) known to be important for CaM C-lobe binding (35, 38, 39) to double alanines (I375A/Q376A or IQ/AA). Analysis of FRET results between CaM and KCNQ1-VenHAB-IQ/AA revealed negligible FRET signals beyond those observed with negative controls (Fig. 1F, red, and Fig. S1C and D), consistent with the lack of binding between CaM and KCNQ1-IQ/AA. The lack of FRET signal is not due to lack of KCNQ1-IQ/AA translation, as cells expressing KCNQ1-VenHAB-IQ/AA still exhibited robust Venus fluorescence intensity (Fig. S3A). Taken together, our FRET assay detected robust binding between CaM and KCNQ1 WT as well as no interactions between CaM and KCNQ1-IQ/AA designed to ablate CaM binding to KCNQ1. These results validated our assay for probing interactions between CaM variants and the full-length KCNQ1 channel in live cells. We note that fluorophore fusion to KCNQ1 and CaM may induce possible steric effects on KCNQ1/CaM interactions. However, this effect would consistently apply to all CaM variants as the fluorophores were tagged in the same location, thereby allowing comparisons for differences in binding.

CaM variants interact with KCNQ1 with different affinities

We next applied our FRET-based assay to probe whether CaM variants bind to the full-length KCNQ1 differently compared with CaM WT. We generated 14 Cerulean-tagged CaM missense

variants, including 13 arrhythmia-linked variants (E46K, N54I, N98S, A103V, E105A, G114W, D130G, D132H, D132N, D134H, Q136P, E141G, and F142L) and 1 non-arrhythmia-linked variant identified in the gnomAD database (Q50R) (17, 54). FRET measurements were performed between each CaM variant and KCNQ1-VenHAB cotransfected in CHO cells under resting or “basal” intracellular $[Ca^{2+}]$ conditions. The “basal” intracellular $[Ca^{2+}]$ condition was designed to mimic resting low $[Ca^{2+}]$ during cardiac diastole and was attained by imaging CHO cells incubated in Hanks’ balanced salt solution (HBSS) solutions containing 1.25 mM Ca^{2+} . We then fitted an estimated $K_{D,eff}$ and constructed the 95% CI by bootstrapping for each of the CaM variants (Fig. 2, Fig. S4, and Table S1). Statistical significance in binding affinities were determined if the 95% CI of the CaM variant did not overlap with that of the WT control. Our screening identified four CaM variants (E46K, G114W, F142L, and Q50R) which exhibited statistically significant decreased binding affinity to KCNQ1 (increased $K_{D,eff}$) when compared with CaM WT (Fig. 2A and C). The CaM E46K variant featured a substantial reduction in binding affinity ($K_{D,eff} = 70.23$ AU E46K vs. 30.2 AU WT). Although the reduction in binding is significant, the modest 2.6-fold decrease in affinity suggests that KCNQ1 channels in cardiomyocytes may still preassociate with CaM E46K depending on the relative concentrations of the CaM E46K variant vs. WT. In contrast, the CaM G114W variant exhibited greatly diminished binding to KCNQ1 (Fig. 2A). We were unable to obtain a reliable $K_{D,eff}$ estimate between CaM G114W and KCNQ1 due to the minimal rise in E_D signals (Fig. 2A), with the best estimate indicating at least two orders of magnitude increase in $K_{D,eff}$. The lack of FRET signal is not due to a lack of CaM G114W expression, as cells expressing Cerulean-tagged CaM WT and CaM G114W both showed robust Cerulean fluorescence intensities (Fig. S3B). The FRET result indicates KCNQ1 channels in cardiomyocytes carrying the CaM G114W variant are likely devoid of CaM G114W and are instead endowed with CaM WT. Structurally, neither CaM E46 nor G114 is a direct Ca^{2+} -coordinating residue. CaM E46 is located within the N-lobe EF1-EF2 linker while CaM G114 is situated within the C-lobe EF3-EF4 linker (Fig. 1C). Their positions suggest that CaM E46K and G114W likely disrupt CaM/KCNQ1 binding by altering N-lobe interaction with HB and C-lobe interaction with HA, respectively. However, potential allosteric effects of each variant on the opposing lobe cannot be ruled out.

The majority of variants analyzed (10/14) demonstrated similar or better binding affinity to KCNQ1 when compared with CaM WT under basal intracellular $[Ca^{2+}]$ conditions. Two variants (E105A and D130G) exhibited significantly smaller $K_{D,eff}$ estimates indicating enhanced binding affinity to KCNQ1 compared with WT (Fig. 2A, C). The remaining variants such as CaM N54I or CaM A103V yielded similar $K_{D,eff}$ estimates compared with WT (Fig. 2A, C). Taken together, these results demonstrate that most CaM variants can sufficiently compete with their WT counterpart and interact with KCNQ1 in a dominant negative manner. Even among the variants with reduced binding, CaM E46K only showed a mild 2.6-fold reduction. Our screening included variants in multiple CaM regions in both N- and C-lobes, suggesting KCNQ1/CaM interaction is generally tolerant of single missense mutation throughout CaM.

The results so far show that most CaM variants can compete with CaM WT for binding KCNQ1 in a live-cell context under basal intracellular $[Ca^{2+}]$ conditions. In the cardiac cycle, CaM can coordinate Ca^{2+} ions and change conformation when intracellular $[Ca^{2+}]$ rises during systole, thereby potentially changing CaM interaction with KCNQ1. We therefore undertook additional

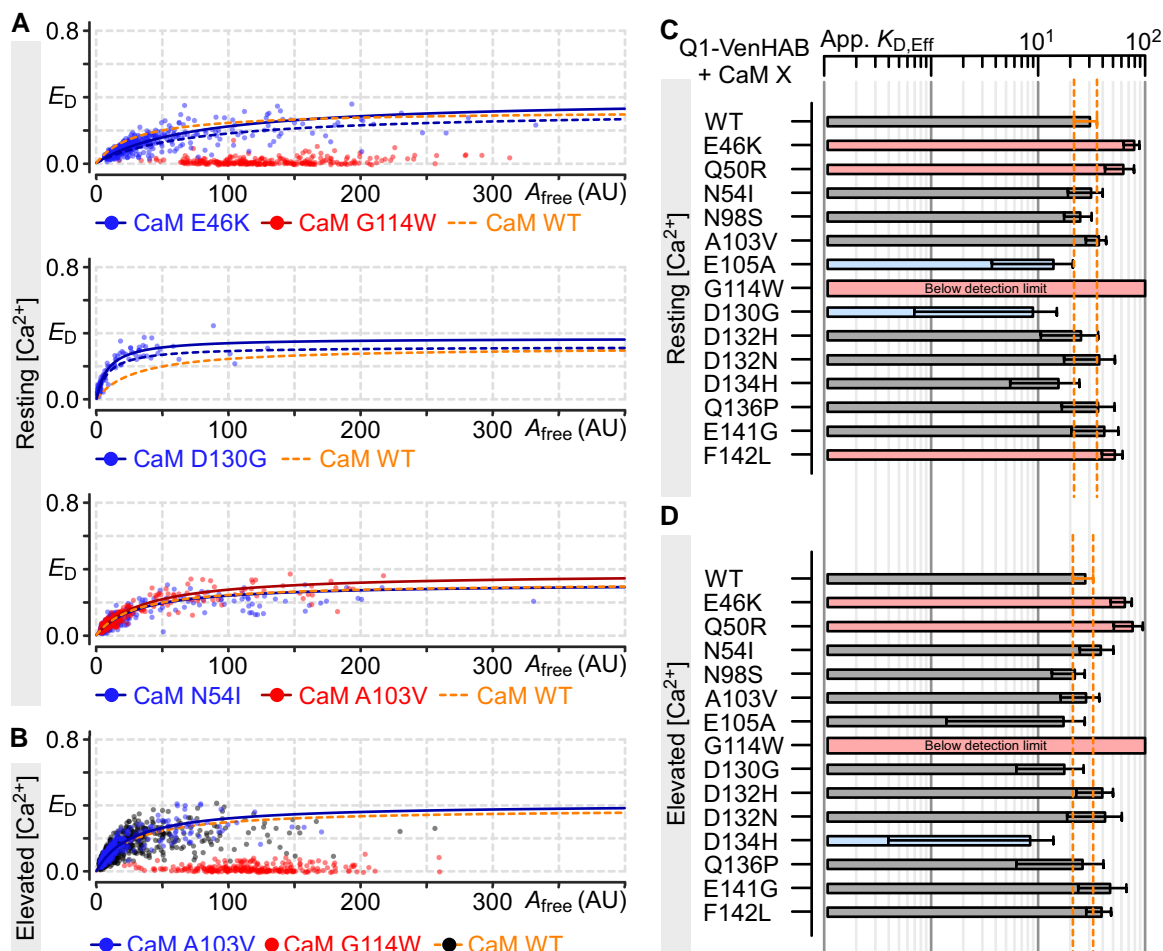


Fig. 2. Arrhythmia-associated CaM variants binding to full-length KCNQ1 in live cells. A) FRET binding curves measured between KCNQ1-VenHAB and Cerulean-tagged CaM variants as labeled under resting Ca^{2+} conditions. Each dot is one cell. Dotted blue lines are the FRET binding curves with E_{Max} normalized to the same level as WT for $K_{D,eff}$ comparison. Top, middle, and bottom plots illustrate variants exhibiting decreased, increased, and similar binding affinity to KCNQ1-VenHAB, respectively. A_{free} corresponds to estimated free concentration of KCNQ1-VenHAB. $n = 708$ (E46K), 291 (G114W), 244 (D130G), 623 (N54I), and 686 (A103V). B) Format as in A but showing FRET binding curves measured under elevated Ca^{2+} conditions. $n = 292$ (G114W) and 622 (A103V). C and D) Bar plot summary for fitted $K_{D,eff}$ between KCNQ1-VenHAB and the indicated CaM variant under resting or elevated Ca^{2+} conditions. Colored (red and blue) bars indicate CaM variants with significantly different $K_{D,eff}$ compared with WT. Error bars are 95% CI. Orange dotted lines denote 95% CI for WT. See Tables S1 and S2 for all fitted binding curve parameters.

FRET experiments with CaM WT and variants under elevated intracellular $[Ca^{2+}]$ conditions to explore potential Ca^{2+} -dependent effects. To this end, we incubated transfected CHO cells in solutions containing 10 mM Ca^{2+} and 4 μ M ionomycin for at least 15 min prior to imaging. This “high” $[Ca^{2+}]$ condition was designed to saturate intracellular $[Ca^{2+}]$ beyond levels experienced during cardiac systole. We note that we do not explicitly measure intracellular $[Ca^{2+}]$ with this method, and it is possible for local microdomain $[Ca^{2+}]$ to affect CaM binding to KCNQ1. FRET binding curves obtained between KCNQ1-VenHAB and Cerulean-tagged CaM WT revealed similar binding affinity ($K_{D,eff} = 27.3$ AU) compared with basal Ca^{2+} conditions ($K_{D,eff} = 30.2$ AU) (Fig. 2B, D), suggesting that CaM binding affinity to KCNQ1 may not change dramatically between diastole and systole in a cardiomyocyte. Our finding that CaM binding to KCNQ1 is not significantly affected by raising intracellular $[Ca^{2+}]$ is consistent with prior studies demonstrating that I_{Ks} ionic current is maximally activated over physiological ranges of intracellular $[Ca^{2+}]$ (40, 41). Next, we performed FRET binding analysis of the CaM variants which generally yielded the same trends as those seen in basal $[Ca^{2+}]$ conditions, with most variants exhibiting

similar or stronger binding affinity to KCNQ1 (Fig. 2D, Fig. S5, and Table S2). Among the variants with reduced binding in the basal $[Ca^{2+}]$ conditions, the CaM G114W variant maintained a severe loss of interaction with KCNQ1 (Fig. 2B). This finding indicates that the CaM G114W likely does not associate with KCNQ1 at any point during the cardiac cycle. Similarly, the CaM E46K variant featured roughly 2-fold reduced binding affinity ($K_{D,eff} = 63.1$ AU) compared with WT in high $[Ca^{2+}]$ conditions, mirroring the results seen in basal $[Ca^{2+}]$ conditions. This suggests that CaM E46K association to KCNQ1 is also likely unaffected by calcium cycling within cardiomyocytes. Curiously, we found one variant, CaM F142L, which showed statistically significant reduced affinity to KCNQ1 under basal Ca^{2+} conditions, but no significant difference compared with WT under high Ca^{2+} conditions (Fig. 2B, D). This suggests that CaM F142L may interact with KCNQ1 in a Ca^{2+} -dependent manner with variable binding depending on intracellular $[Ca^{2+}]$ during the cardiac cycle. Interestingly, CaM F142L has been previously found to exhibit abnormal Ca^{2+} -dependent affinity to the $Ca_v1.2$ IQ domain (33). We further found another variant, CaM E105A, which showed enhanced affinity to KCNQ1 under basal Ca^{2+} conditions but unchanged affinity compared

with WT under high Ca^{2+} conditions (Fig. 2B, D). However, $K_{D,\text{Eff}}$ calculated for CaM E105A between resting and elevated Ca^{2+} conditions does not differ significantly. CaM E105A therefore likely does not exhibit enhanced binding to KCNQ1 compared with CaM WT. For most variants, such as CaM A103V, there were no significant differences for CaM variant binding affinity to KCNQ1 under high Ca^{2+} conditions when compared with WT (Fig. 2B, D). Taking the combined FRET results together, our findings suggest that most CaM variants feature WT-like binding affinity to KCNQ1 over physiological ranges of intracellular $[\text{Ca}^{2+}]$. As these variants are capable of preassociation to KCNQ1, our findings further delineate the CaM variants which may confer KCNQ1 current dysfunction in cardiomyocytes.

Effect of CaM variants on KCNQ1 membrane trafficking

Given the finding that most CaM variants feature similar binding affinity to KCNQ1 as CaM WT, we next investigated how CaM variants association to KCNQ1 may affect current conduction. Previous studies have shown that CaM facilitates KCNQ1 biogenesis and trafficking to the plasma membrane (5, 6). Thus, CaM variants may modulate current amplitude by affecting channel membrane trafficking. To explore this possibility, we developed a fluorescence-based assay to compare KCNQ1 membrane trafficking efficiency when coexpressed with CaM variants vs. CaM WT. We generated a pseudo-WT (psWT) KCNQ1 construct in which a Cerulean is tagged to the carboxy-terminus and a hemagglutinin (HA) tag is inserted within the extracellular S1-S2 linker between E146 and Q147 (Fig. 3A, KCNQ1-psWT-HA-Cer). The extracellular HA tag enabled targeted fluorescence labeling of KCNQ1 channels on the plasma membrane with an Alexa Fluor 594 (Alexa-594) fluorophore. In contrast, the carboxy-terminus-labeled Cerulean afforded an estimation for the total number of KCNQ1 channels within each cell. In each cell transfected with this construct, we defined an apparent trafficking efficiency metric by the fluorescence intensity ratio of Alexa-594 (plasma membrane-bound KCNQ1) to Cerulean (total KCNQ1),

$$\text{Apparent trafficking efficiency} = \frac{S(\text{Alexa-594})}{S(\text{Cerulean})}.$$

In this assay, we cotransfected CHO cells with KCNQ1-psWT-HA-Cer with CaM WT. Thirty-six hours after transfection, the plasma membrane-bound channels were labeled with a primary anti-HA antibody followed by an Alexa-594 secondary antibody. During staining with the anti-HA antibody, the cells were fixed but not permeabilized through PFA fixation, thus ensuring Alexa-594 was only conjugated on the plasma membrane-bound KCNQ1. The cells were then imaged by confocal microscopy, which revealed robust Cerulean and Alexa-594 fluorescence (Fig. 3B, top 2 panels). Cerulean signal could be seen throughout the cells, while Alexa-594 signals were most evident at the cell membrane, suggesting specific Alexa-594 labeling of membrane-bound channels. Similar fluorescence measurements over 226 cells and revealed an apparent trafficking efficiency of 0.171 ± 0.010 AU (mean \pm SEM), establishing a baseline value to which we can compare potential CaM variants effect on KCNQ1 trafficking (Fig. 3C, light gray dot). For negative control, we cotransfected CHO cells with Cerulean-tagged KCNQ1 without HA tags in the S1-S2 linker (KCNQ1-psWT-Cer) and performed the same Alexa-594 staining. Confocal imaging of these constructs revealed robust cerulean intensity but minimal Alexa-594 signals (Fig. 3B, second row). The

apparent trafficking efficiency computed for this negative control construct over 200 cells was 0.076 ± 0.005 AU (Fig. 3C), demonstrating a clear decrease in our trafficking efficiency metric.

With our assay, we next tested how arrhythmia-associated CaM variants may affect KCNQ1 membrane trafficking by measuring the apparent trafficking efficiency of KCNQ1-HA-Cer cotransfected with various CaM variants (Fig. 3B and C). Significant differences in membrane trafficking were determined by one-way ANOVA followed by Dunnett's test. We found that seven CaM variants (Q50R, N54I, A103V, E105A, D132H, D132N, and E141G) had no effect on KCNQ1 trafficking efficiency compared with CaM WT (Fig. 3C and Table S3). As CaM N54I, A103V, D132H, D132N, and E141G exhibited similar binding affinity to KCNQ1 compared with CaM WT (Fig. 2C), the trafficking assay data indicate that these variants likely do not contribute to arrhythmia by modifying I_{Ks} or KCNQ1 current amplitude through changing channel trafficking efficiency.

On the other hand, we found three CaM variants (E46K, F90L, and D132E) that reduced KCNQ1 trafficking efficiency compared with CaM WT (Fig. 3B and C and Table S3). CaM E46K and F90L exhibited mean apparent trafficking efficiency of 0.121 and 0.114 AU, respectively, representing ~ 0.47 -fold and 0.4 -fold decreased membrane trafficking compared with WT. These findings suggest that these variants may contribute to arrhythmogenesis in part by reducing I_{Ks} or KCNQ1 current amplitude in cardiomyocytes.

Lastly, we found five CaM variants (D96V, G114W, D130G, D134H, and Q136P) increased KCNQ1 trafficking efficiency compared with CaM WT (Fig. 3B and C and Table S3). The variants D134H and Q136P have an apparent trafficking efficiency of 0.243 and 0.246 AU or ~ 1.75 -fold increase trafficking efficiency compared with WT. As D134H and Q136P bind KCNQ1 with similar affinity as CaM WT, these results suggest that these mutants may contribute to arrhythmogenesis in part by increasing I_{Ks} of KCNQ1 current amplitude. Compared with D134H and Q136P, CaM G114W had a striking apparent trafficking efficiency of 0.324 AU or 2.6-fold increase compared with WT (Fig. 3B and C). The finding that CaM G114W, which exhibits minimal binding to KCNQ1 (Fig. 2C), increased KCNQ1 trafficking efficiency is interesting. To explore the possibility that this effect is an artifact of CaM overexpression in our assay, we repeated the trafficking assay under endogenous CaM, overexpressed CaM WT, and overexpressed CaM G114W conditions. We found that CaM WT overexpression led to a trend in higher KCNQ1 trafficking compared with endogenous CaM conditions but does not reach statistical significance (Fig. S6). In contrast, CaM G114W overexpression induced a statistically significant increase in KCNQ1 trafficking compared with endogenous CaM conditions (Fig. S6). These data suggest that CaM G114W induces an increase in KCNQ1 trafficking independent of CaM overexpression in our system. This effect is also likely not due to strong CaM G114W overexpression compared with WT, as Cerulean-tagged CaM G114W did not exhibit higher fluorescence intensity compared with CaM WT (Fig. S3B). Possible mechanisms by which CaM G114W may increase KCNQ1 trafficking are presented in the discussion. In all, the trafficking assay data delineate the arrhythmia-associated CaM variants that affect KCNQ1 membrane trafficking efficiency, which may alter total I_{Ks} or KCNQ1 current amplitude to contribute to arrhythmogenesis.

Select CaM variants affect baseline KCNQ1 current activation kinetics

In addition to modulating KCNQ1 membrane trafficking, CaM is also known to affect KCNQ1 gating (5, 10). Previous studies have

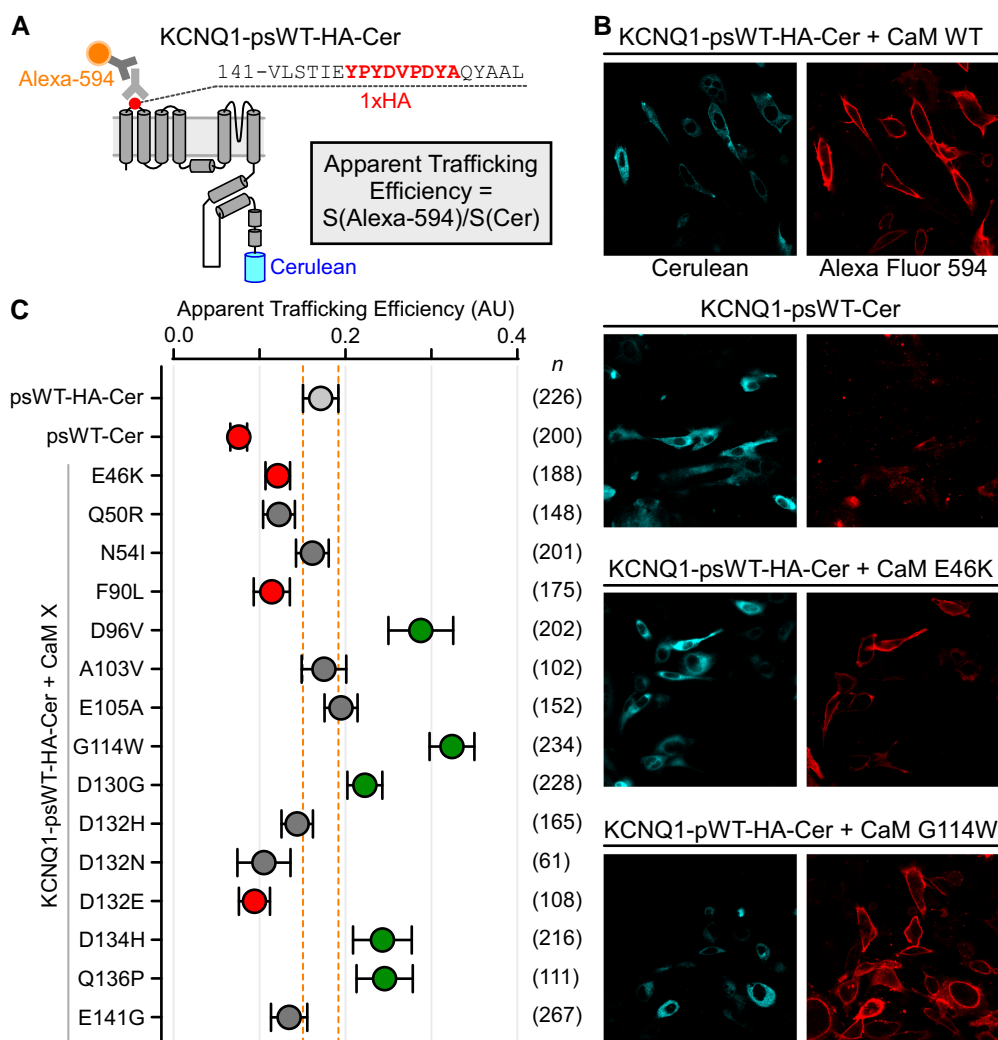


Fig. 3. Effect of CaM variants on KCNQ1 membrane trafficking. A) Cartoon illustration of KCNQ1 construct used for membrane trafficking assay (KCNQ1-psWT-HA-Cer). Cerulean fluorophore and HA tag were inserted into KCNQ1 as diagrammed. Total KCNQ1 expressed within the cell correlates with Cerulean signal, while membrane-trafficked KCNQ1 was estimated with Alexa-594 signal. An apparent trafficking efficiency for each cell was derived by dividing the Alexa-594 signal to that of Cerulean on confocal microscopy. B) Confocal microscopy images of KCNQ1-psWT-HA-Cer coexpressed with CaM; left cyan and right red images show Cerulean and Alexa-594 signals, respectively. KCNQ1-psWT-Cer is a construct with a Cerulean fused to the carboxy-terminus but no HA tag in the S1-S2 linker. C) Summary data for apparent trafficking efficiency for KCNQ1 coexpressed with different CaM variants. Each dot indicates the mean and error bars represent 95% CI. Dashed lines denote 95% CI for WT control. *n* indicates number of cells analyzed for the corresponding CaM variant. Green (right side) and red (left side) denote statistically significant increased and decreased membrane trafficking when compared with WT control, respectively. Statistical significance calculated with one-way ANOVA followed by Dunnett's test. See Table S3 for all parameters.

shown that CaM tunes KCNQ1 function by modulating baseline current activation kinetics by controlling channel entry into the fully activated open state independent of intracellular Ca^{2+} (10). Given the numerous CaM variants exhibiting WT-like interaction with KCNQ1, some of the CaM variants may disrupt KCNQ1 baseline function leading to arrhythmogenesis observed in variant carriers. To examine this possibility, we undertook TEVC experiments in *Xenopus* oocytes. In contrast to the FRET experiments, TEVC was performed with unlabeled KCNQ1 and CaM to avoid potential artifact related to fluorophore fusion. The *Xenopus* oocyte system further enabled direct injection of RNA encoding KCNQ1 and CaM variants, side-stepping potential cotransfection issues in mammalian cell lines. We did not suppress endogenous CaM in *Xenopus* oocyte, which shares 100% amino acid identity with human CaM. Furthermore, CaM variants are cotranslated with CaM WT in cardiomyocytes in vivo. Figure 4A illustrates exemplar ionic

current recorded when KCNQ1 was coexpressed with CaM WT and subjected to a series of test voltage pulses. At higher depolarizing pulses, KCNQ1 current featured two distinct time-dependent components of activation (Fig. 4A, red arrow), fast and slow. These two components have been previously shown to approximate KCNQ1 entry into distinct open states (55). We next screened KCNQ1 coexpressed with CaM variants studied in our FRET assay with TEVC. We replaced the CaM N98S and F142L variants in the TEVC screen with the CaM N98I and D132E variants, as the former two have been previously reported in the context of KCNQ1 (10, 35).

We first analyzed KCNQ1 steady-state activation property when coexpressed with different CaM variants by fitting the conductance-voltage (G - V) relationship for the half-activation voltages ($V_{1/2}$), which is the membrane voltage at which KCNQ1 channels are half maximally activated. Statistical significance

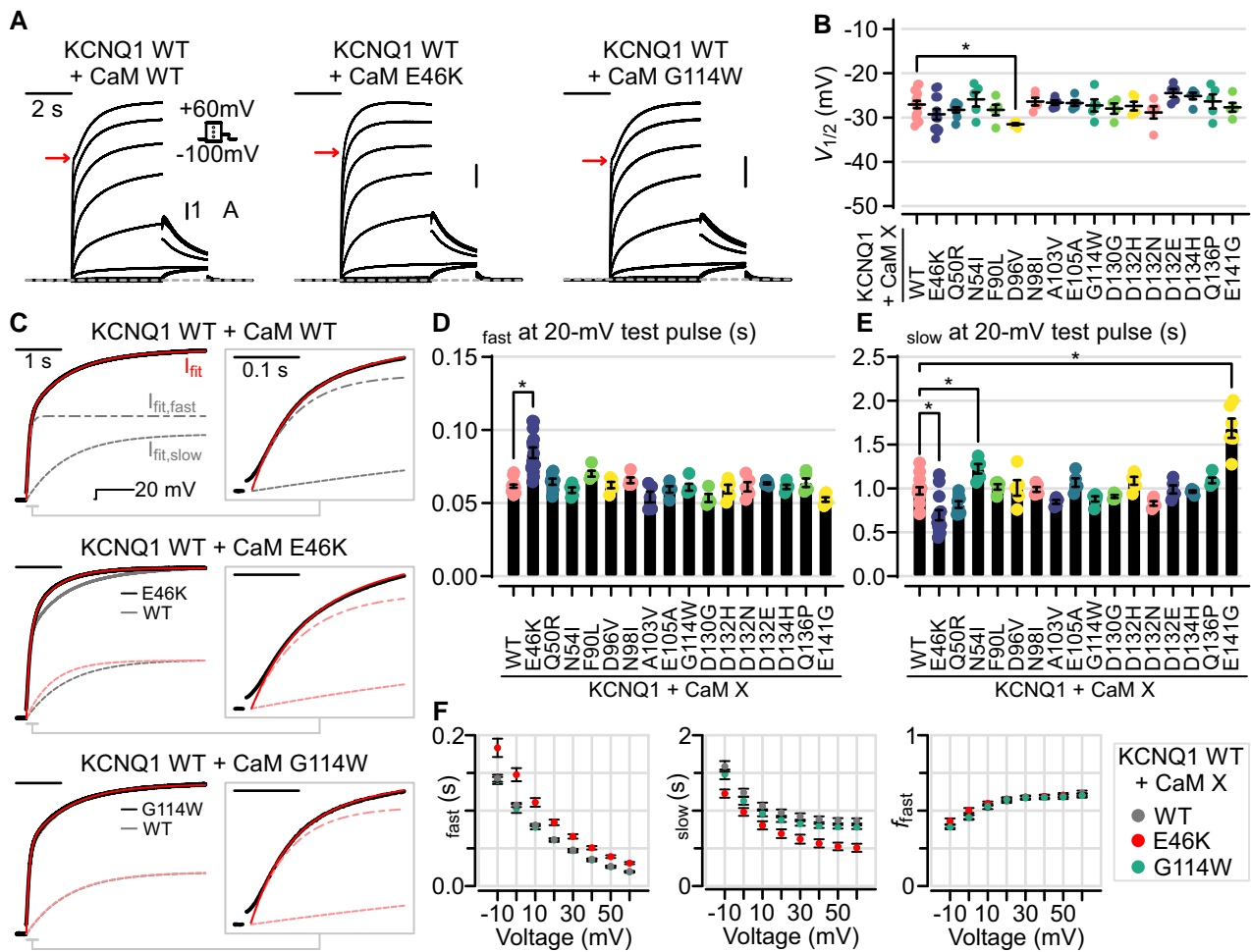


Fig. 4. Arrhythmia-associated CaM variants effect on baseline KCNQ1 steady-state activation and activation kinetics. A) Exemplar currents recorded from KCNQ1 WT coexpressed with either CaM WT or CaM variants. B) Summary half-activation voltage ($V_{1/2}$) of the G-V curves for KCNQ1 when coexpressed with various CaM variants. C) Exemplar biexponential fitting for KCNQ1 activation kinetics. D and E) Summary bar plots for fitted fast and slow time constants for KCNQ1 coexpressed with CaM variants when tested at 20 mV. F) Biexponential fitting parameters for KCNQ1 WT coexpressed with CaM WT, E46K, and G114W as a function of voltage. All error bars are SEM.

for all fitted parameters were determined by ANOVA followed by Dunnett's test. Analysis of measured $V_{1/2}$ showed minor differences between WT and all CaM variants probed (Fig. 4B and Table S4). CaM D96V demonstrated a subtle but statistically significant 4.4 mV hyperpolarizing shift in $V_{1/2}$ (adjusted P -value 0.037). All other variants tested revealed no differences in $V_{1/2}$ compared with WT control. These results indicate that most CaM variants do not dramatically perturb the baseline ability of KCNQ1 to open at steady state.

Beyond steady-state response, CaM has been shown to modulate KCNQ1 activation kinetics (10). As potassium current activation kinetics figure critically in action potential duration, we next quantified current activation kinetics at 20 mV depolarization by fitting the current tracings to a biexponential function with fast and slow components (τ_{fast} and τ_{slow}). As shown in Fig. 4C, KCNQ1 WT coexpressed with CaM WT yielded ionic currents well-fitted by a biexponential function when depolarized to 20 mV (red fit vs. black current tracing). We next performed the same biexponential fitting procedure on KCNQ1 activation kinetics at 20 mV depolarization when coexpressed with CaM variants (Fig. 4C-E). This analysis revealed that the CaM E46K variant significantly affected KCNQ1 current activation. Specifically, CaM E46K induced a lengthening of τ_{fast} (0.062 WT vs. 0.084 E46K, adjusted P -value

<0.0001) and a reduction of τ_{slow} (0.973 WT vs. 0.695 E46K, adjusted P -value <0.0001) when compared with WT (Fig. 4C-E). These two effects together decelerated the fast component and accelerated the slow component, yielding a more rounded appearance for current activation kinetics (Fig. 4A, red arrow). The reduction in τ_{slow} dominated in a 20 mV 4 s test pulse, with KCNQ1 + CaM E46K current reaching steady-state more rapidly than WT as shown by normalized current superposition (Fig. 4C, solid black vs. gray). To further test whether E46K affected activation, we performed kinetics fitting at various test voltages and found that it induced consistent increases in τ_{fast} and decreases in τ_{slow} for test voltages ranging from -10 to +60 mV (Fig. 4F), providing additional validation for CaM E46K effect on KCNQ1 kinetics. Analysis of other CaM variants revealed that CaM variants N54I and E141G significantly increased τ_{slow} but spared τ_{fast} at 20 mV (Fig. 4E), indicating that CaM N54I and E141G slow KCNQ1 current onset upon membrane depolarization. The ability of the CaM E46K, N54I, and E141G variants to modulate the slow kinetics component is consistent with prior studies demonstrating a role for CaM in modulating the KCNQ1 activation (10).

The remaining CaM variants assayed did not yield significant kinetics changes compared with WT at 20 mV (Fig. 4D and E). Notably, the CaM G114W variant induced no changes in either

τ_{fast} or τ_{slow} when the test pulse ranged from -10 to $+60$ mV (Fig. 4C–F). As CaM G114W variant features severely reduced binding to KCNQ1, this finding is consistent with the idea that CaM G114W cannot compete with CaM WT for KCNQ1, leading to the channel associating with endogenous CaM WT and exhibiting WT behavior.

Taken together, our results suggest that CaM modulation of KCNQ1 kinetics may be physiologically relevant and further delineate CaM variants that can modulate baseline KCNQ1 current. These kinetic alterations may interact nonlinearly in the cardiac action potential to contribute to arrhythmogenesis.

Select CaM variants affect baseline I_{Ks} current activation kinetics

Although the KCNQ1–CaM complex constitutes a fully functional voltage-dependent channel, KCNQ1 additionally interacts with the auxiliary subunit KCNE1 in cardiomyocytes to conduct the slow delayed rectifier current (I_{Ks}) (36, 37, 56). We will refer to the KCNQ1 + KCNE1 complex as I_{Ks} . Functionally, KCNE1 causes a significant depolarizing shift in the KCNQ1 steady-state $V_{1/2}$ and strongly decelerates current activation kinetics (Fig. 5A), both important factors in the physiological role of I_{Ks} . Given the importance of KCNE1 association to KCNQ1 in cardiomyocytes, we undertook additional TEVC analysis to probe how KCNE1 may alter the ability of CaM variants to modulate baseline KCNQ1 current.

As in the prior KCNQ1 experiments, we first analyzed I_{Ks} steady-state activation when coexpressed with CaM variants in *Xenopus* oocytes. Similar to the results seen in the KCNQ1-only screen, all CaM variants screened exerted minor effects on I_{Ks} baseline half-activation voltage (Fig. 5B and Table S5). CaM D96V variant induced a subtle 7.26 mV hyperpolarizing shift in the $V_{1/2}$ of I_{Ks} (adjusted P -value 0.034 by one-way ANOVA and Dunnett's test), mirroring the trend seen in the KCNQ1-only screen. All other CaM variants screened did not show statistically significant differences in I_{Ks} $V_{1/2}$ when compared with WT control (Fig. 5B). The comparable effects of CaM variants on KCNQ1 with and without KCNE1 coexpression suggest that KCNE1 does not confer additional ability for these CaM variants to modulate channel opening at steady state.

We next examined whether CaM variants modulate I_{Ks} activation kinetics by fitting the ionic currents with a single exponential function when depolarized to 30 mV. As I_{Ks} activates with a significant delay that cannot be fitted by an exponential function in the early phase, our fits incorporated a time lag (t_{Lag}) before which the current data were not fitted (Fig. 5C, gray normalized ionic current and red fit) as in prior studies (57). Kinetics fitting of I_{Ks} coexpressed with CaM WT revealed an activation time constant (τ) of 3.52 ± 0.24 s (mean \pm SEM) at 30 mV (Fig. 5C–E). Next, the same fitting procedure was repeated for I_{Ks} coexpressed with CaM variants as summarized in Fig. 5E, revealing three CaM variants (N54I, Q136P, and E141G) that significantly prolonged activation kinetics when compared with WT (adjusted P -values < 0.0001 , 0.028, and 0.0026 for N54I, Q136P, and E141G, respectively). CaM E141G increased the activation τ of I_{Ks} to 6.17 ± 0.96 s when depolarized to 30 mV, ~ 1.75 -fold increase over that of WT and can be appreciated by comparison of normalized currents (Fig. 5C, left panel). Additional kinetics fitting of different step voltages from 30 to 100 mV further revealed a consistent increase in τ when I_{Ks} is coexpressed with CaM N54I and E141G when compared with WT (Fig. 5D). Interestingly, CaM N54I and E141G also significantly increased τ_{slow} when coexpressed with KCNQ1 without KCNE1

(Fig. 4E). Taken together, these results suggest that CaM N54I and E141G may slow KCNQ1 and I_{Ks} activation kinetics by a similar mechanism. On the other hand, CaM Q136P did not significantly affect activation kinetics of KCNQ1 without KCNE1 (Fig. 4E) but had an effect on I_{Ks} kinetics (Fig. 5E), suggesting that CaM Q136P requires KCNE1 association to perturb channel gating.

In contrast, the remaining CaM variants did not affect I_{Ks} activation kinetics at 30 mV (Fig. 5E). In particular, CaM G114W did not alter I_{Ks} activation kinetics over voltage ranges from 30 to 100 mV (Fig. 5C and D). This result is further consistent with the idea that CaM G114W cannot associate with the channel carboxy-terminus; thus, the membrane-trafficked I_{Ks} are endowed with endogenous CaM WT and exhibit WT behavior. Another notable variant is CaM E46K, which induced a decrease in τ_{slow} or hastening of current kinetics in KCNQ1 without KCNE1 (Fig. 4E). Kinetics fitting for I_{Ks} coexpressed with CaM E46K revealed a trend of hastened activation kinetics (mean $\tau = 2.88$ vs. 3.52 s for CaM E46K vs. CaM WT at 30 mV) consistent with the effects seen in KCNQ1 without KCNE1 but ultimately did not reach statistical significance after controlling for multiple comparisons (Fig. 5E). These findings suggest KCNE1 may blunt CaM E46K effect on KCNQ1 activation kinetics, rendering the kinetics effect on I_{Ks} more subtle compared with KCNQ1 alone.

Altogether, our functional screen demonstrates that select CaM variants can modulate baseline I_{Ks} function, with most significant effect on activation kinetics. Moreover, comparison between the I_{Ks} and KCNQ1 results generally demonstrates consistent effects by CaM variants N54I, D96V, and E141G, identifying CaM variants that can affect KCNQ1 gating regardless of KCNE1 association. Our functional screen thus delineates CaM variants (N54I, Q136P, and E141G) that can modulate I_{Ks} baseline activation kinetics under resting intracellular Ca^{2+} conditions. As the speed of I_{Ks} activation aids in controlling the cardiac action potential duration, these CaM variant-induced changes in I_{Ks} function may work in concert with effects on other CaM targets to cause arrhythmia.

Discussion

Missense variants in CaM have emerged in recent years to underlie severe arrhythmia with high mortality rate (14, 16–20). As CaM targets numerous ion channels important to the cardiac action potential, the mechanisms of CaM-induced arrhythmia (“calmodulinopathy”) are necessarily complex. Multiple studies have shown that CaM variants can significantly impact $\text{Ca}_v1.2$ and/or RyR2 function (14, 16–18, 23, 26, 27, 29, 30, 32–34, 58). In contrast, although CaM also associates and regulates KCNQ1 channel membrane trafficking and function, relatively little is known regarding whether KCNQ1 or I_{Ks} dysfunction may also contribute to calmodulinopathy. Here, we applied extensive live-cell FRET binding assays, fluorescence-based membrane trafficking assays, and functional electrophysiology to contextualize KCNQ1 within CaM-induced arrhythmogenesis (Fig. 6).

Most CaM variants can sufficiently compete with CaM WT for binding to KCNQ1

As three independent genes encode CaM within the human genome, CaM variants likely compete with endogenous CaM WT for binding to KCNQ1 within cardiomyocytes. In this study, we examined whether a CaM variant may sufficiently compete with CaM WT with a FRET-based assay that quantify CaM variants binding to KCNQ1 in live cells. Because CaM is also known to interact

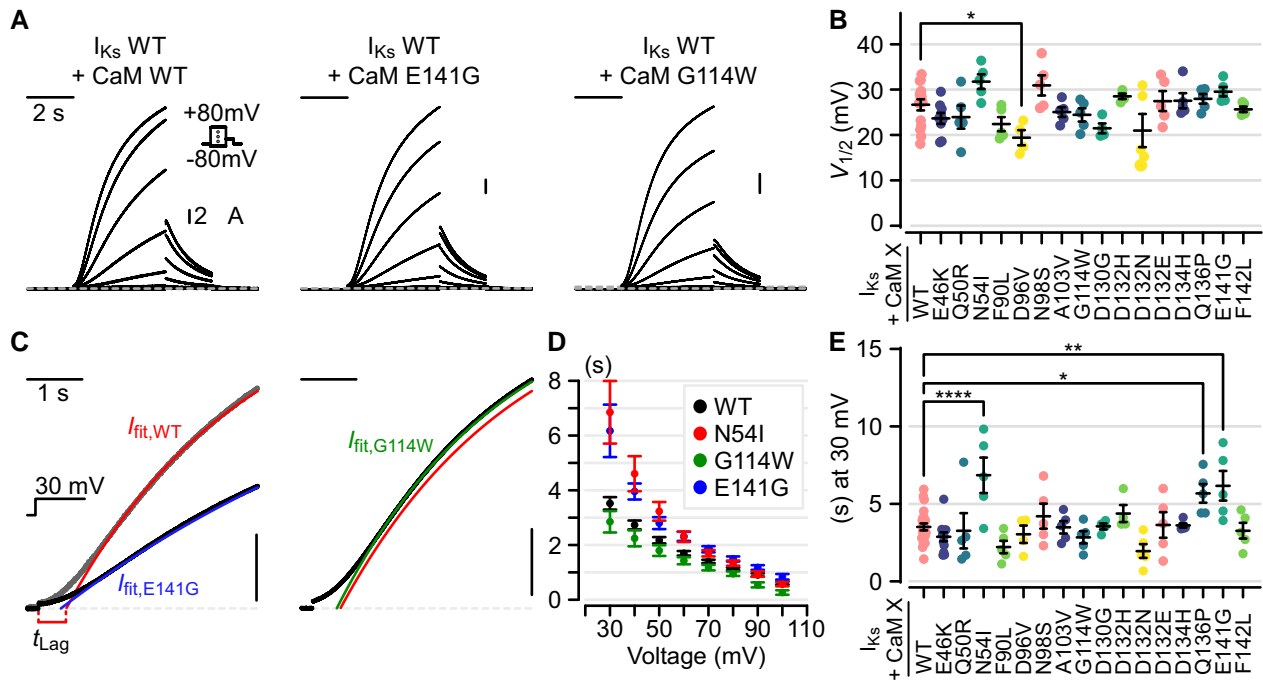


Fig. 5. Arrhythmia-associated CaM variants effect on I_{Ks} (KCNQ1 + KCNE1) steady-state activation and activation kinetics. A) Exemplar I_{Ks} recordings from *Xenopus* oocytes when coexpressed with CaM WT, E141G, or G114W. B) Summary activation $V_{1/2}$ fitted in G–V curves for I_{Ks} coexpressed with CaM variants. Statistical significance determined by one-way ANOVA and Dunnett’s test. C) Exemplar activation kinetics fitting for I_{Ks} coexpressed with CaM variants when depolarized to 30 mV. Currents were fitted to the equation $I(t) = A \cdot \exp(-(t - t_{lag})/\tau)$, with points prior to t_{lag} excluded from the fitting procedure. Plotted ionic currents were normalized to the fitted A for comparison. Vertical scale bars show 25% of normalized current. Left panel: gray and black represent normalized ionic current for I_{Ks} coexpressed with CaM WT and E141G, respectively. Right panel: black and green indicate normalized ionic current and kinetics fit for I_{Ks} coexpressed with CaM E141G. Red line shows identical WT fit seen in the left panel. D) Fitted activation time constant for I_{Ks} coexpressed with CaM WT, N54I, G114W, and E141G as a function of step voltage from 30 to 100 mV. Error bars are SEM. E) Summary of fitted activation time constant for I_{Ks} coexpressed with CaM WT or variants when depolarized to 30 mV. Significance was determined by one-way ANOVA followed by Dunnett’s test.

with multiple KCNQ1 domains including the voltage-sensing domain, a key strength of our assay is quantification of CaM interaction with the full-length KCNQ1 channel. Our FRET-based screen demonstrates that most CaM variants (10/14 screened) interact with the full-length KCNQ1 with similar or better affinity compared with CaM WT under both resting and elevated intracellular $[Ca^{2+}]$ conditions, suggesting that most CaM variants can preassociate with KCNQ1 in cardiomyocytes expressing both CaM variants and WT (Figs. 2 and 6A). One potential reason that many CaM variants exhibit similar binding affinity to KCNQ1 compared with WT may be because both CaM N-lobe and C-lobe participate in binding KCNQ1 (35, 38, 39, 59). Mutational perturbation of one CaM lobe may be compensated by the other CaM lobe to maintain interaction with KCNQ1. Previous studies have also shown that several CaM variants (e.g. CaM F142L and D96V) bind with similar or higher affinity to other cardiac channels such as $Ca_v1.2$ (29, 33). Specifically, CaM F142L binds the $Ca_v1.2$ IQ domain with WT-like affinity in the Ca^{2+} -bound state but with 10-fold higher affinity over WT in the Ca^{2+} -free state (33). In all, our results extend the propensity for CaM variants to exhibit dominant negative interactions to KCNQ1.

Nevertheless, we identified four CaM variants (E46K, Q50R, G114W, and F142L) that exhibit reduced binding affinity to KCNQ1 when compared with WT (Fig. 6A). Three variants (E46K, Q50R, and F142L) feature mildly reduced binding affinity that could feasibly compete with CaM WT for KCNQ1 depending on the relative concentrations of CaM WT to variant within the cell. In contrast, CaM G114W variant represents an interesting case in that the variant appears to be unable to interact with KCNQ1.

CaM G114W has been previously shown to exhibit impaired binding to RyR2 CaMBD2 and $Ca_v1.2$ IQ domain (27) but not to the extent seen in our data with KCNQ1. Interestingly, CaM G114W features severely impaired binding to the $Na_v1.5$ IQ domain at low intracellular Ca^{2+} levels (60). The varied binding affinities between CaM G114W and distinct CaM targets likely influence which channels are endowed with CaM WT vs. G114W within cardiomyocytes, with the precise distribution representing an important topic for future studies. These binding data collectively also demonstrate the importance of determining CaM variant binding to distinct targets to decipher calmodulinopathy arrhythmogenesis.

CaM variants induce aberrant KCNQ1 membrane expression and current conduction

Our finding that most CaM variants bind to KCNQ1 with similar affinity as CaM WT represents the first step to contextualize KCNQ1’s contribution to calmodulinopathy, as arrhythmia ultimately arises from cardiac action potential pathologies that are triggered by aberrant ionic currents. In KCNQ1, this may be due to the CaM variant effect on channel membrane trafficking or channel gating. We thus undertook extensive fluorescence and electrophysiology experiments in *Xenopus* oocytes and CHO cells to further correlate CaM variant interaction to KCNQ1 with their effects on channel membrane trafficking and function.

With respect to our model systems, we note that the relative concentrations of CaM variants to WT within the cell may lead to differing functional readout. As we found that CaM variants can bind KCNQ1 with varying affinities, the relative ratio of CaM

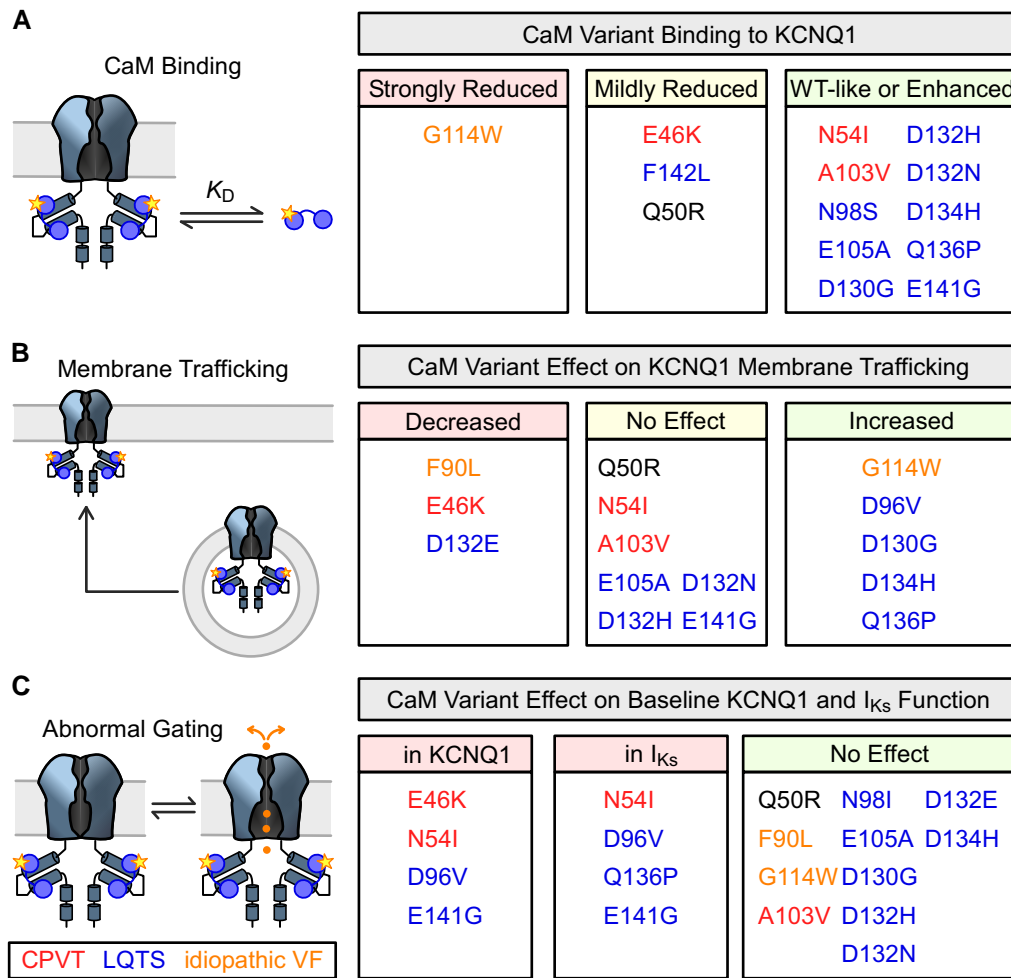


Fig. 6. Summary of the effect of CaM variants on KCNQ1. Classification of CaM variants effect on (A) KCNQ1 binding, (B) KCNQ1 membrane trafficking, and (C) KCNQ1 function. Variants are color-coded by associated arrhythmia: CPVT, red (E46K, N54I, A103V); LQTS, blue (N98S, E105A, D130G, D132H, D132N, D134H, Q136P, E141G, F142L); idiopathic ventricular fibrillation, orange (F90L, G114W); none, black (Q50R).

variants to CaM WT within cardiomyocytes figures critically in whether CaM variants can exert dominant negative effect on KCNQ1 function. The exact CaM WT to variant ratio in native cardiomyocytes still remains undetermined. However, given CaM variant occurs on one out of six alleles, the simplest assumption of balanced expression would suggest the CaM WT to variant ratio is high. Our functional assay in *Xenopus* oocytes, a system known to exhibit high endogenous CaM WT levels, may thus be a suitable system to achieve high CaM WT to variant ratios potentially seen in the pathological state. Still, KCNQ1 dysfunction seen in our assay may be unmasked and suppressed depending on the exact CaM variant to WT ratio in native cardiomyocytes.

As illustrated in Fig. 6B and C, our results identified several CaM variants with effect on KCNQ1 membrane trafficking (E46K, F90L, D96V, G114W, D130G, D132E, D134H, and Q136P) as well as KCNQ1 or I_{Ks} gating (E46K, N54I, D96V, E141G, and Q136P). Given that CaM is well established to be a key regulator for KCNQ1 membrane trafficking and gating (5, 6, 10), these results highlight KCNQ1 dysfunction as an important consideration when elucidating arrhythmogenesis arising from CaM variants.

In particular, the CaM G114W effect on increasing KCNQ1 trafficking is a surprising finding in light of our finding that CaM G114W binds KCNQ1 very poor affinity. CaM binding to KCNQ1 is required for channel assembly and membrane trafficking

(5, 6). Accordingly, CaM G114W is not expected to cause KCNQ1 current dysfunction, as all KCNQ1 expressed on the cardiomyocyte membrane are likely associated with CaM WT. Consistent with this hypothesis, no ionic current abnormalities were detected when KCNQ1 or I_{Ks} were coexpressed with CaM G114W (Fig. 6C). Still, we found that coexpression of KCNQ1 and CaM G114W increased KCNQ1 trafficking efficiency in CHO cells (Fig. 3C and Fig. S6). The mechanism for this observed phenomenon remains unclear. While our experiments suggest CaM G114W overexpression boosts KCNQ1 trafficking independently of overexpression artifacts (Fig. S6), it is possible that some elements of overexpression artifacts remain. As the pool of unbound or free CaM in cardiomyocytes is severely limited to 1% of total CaM (61), it is possible that this phenomenon may be due to redistribution of CaM WT and G114W onto distinct CaM regulatory targets. Another intriguing possibility is that distinct CaM genes may target their corresponding mRNA to distinct cardiomyocyte cellular regions, with studies suggesting *Calml2* mRNA is more favored to spatially cluster with *Ryr2* mRNA (62). Spatial distribution of CaM WT vs. variants within cardiomyocytes to distinct CaM targets may add yet another layer of complexity for how CaM variants affect KCNQ1 membrane expression and function. CaM G114W may also affect KCNQ1 trafficking through an unknown regulatory pathway. Taken together, the CaM G114W variant

highlights the potential complexity of considering distinct CaM targets within the cell, as well as the importance of employing multiple readouts (e.g. binding, membrane trafficking, and functional electrophysiology) to elucidate CaM variant effect.

As KCNQ1 and I_{Ks} activation kinetics mediate cardiac action potential shortening during β -adrenergic stimulation, how do the observed effects in our study correlate to arrhythmia phenotype as color-coded in Fig. 6? We note that caution should be taken when interpreting how CaM-induced KCNQ1 dysfunction translates to the observed clinical phenotype, as CaM variants can affect multiple channels that nonlinearly contribute to the cardiac action potential. This is supported by the observation that LQTS-associated CaM variants do not appear to affect KCNQ1 in a consistent manner (Fig. 6), with distinct variants exerting loss of function, gain of function, or no effects on KCNQ1. The lack of consistent correlation between KCNQ1 dysfunction and phenotype further highlights the need to consider all CaM targets in calmodulinopathy. Nevertheless, CaM variants with effect on KCNQ1 may be more likely to present with stress- or exercise-induced arrhythmia. Select variants further exert KCNQ1 dysfunction consistent with arrhythmia phenotype. For example, the CaM E141G and Q136P variants trigger a slower I_{Ks} activation kinetics compared with WT and may provide less repolarizing current, consistent with their association to LQTS (17). By comparison, the CaM E46K variant induces a faster KCNQ1 activation kinetics and is associated with CPVT. As CPVT is thought to stem from abnormal Ca^{2+} handling during diastole (63), the faster KCNQ1 activation kinetics may contribute to the CPVT phenotype by prolonging diastole. Specifically, KCNQ1 dysfunction caused by CaM E46K may exacerbate the CPVT phenotype during β -adrenergic stimulation where I_{Ks} participates in action potential repolarization. However, CaM E46K is also associated with a reduction in trafficking efficiency, and the activation kinetics effects are more subtle more in I_{Ks} compared with KCNQ1. Adding to the complexity, some variants induce effects seemingly inconsistent with the observed arrhythmia phenotypes. For example, CaM D96V induces a subtle hyperpolarizing shift in KCNQ1 and I_{Ks} steady-state activation as well as increases KCNQ1 trafficking efficiency, both effects expected to increase K^+ flux and shorten the cardiac action potential. Yet, CaM D96V is associated with a LQTS phenotype (17) and a loss of KCNQ1 function would be expected. A likely cause of this difference is that CaM D96V effect on alternate CaM targets such as $Ca_v1.2$ may more prominently drive action potential prolongation in cardiomyocytes compared with its effect on KCNQ1. Thus, the KCNQ1 interaction in this case is protective, and loss-of-function KCNQ1 variants in conjunction with D96V may be especially lethal. Lastly, several CaM variants screened in this study feature WT-like binding affinity to KCNQ1 and minimal effects on KCNQ1 and I_{Ks} channel membrane trafficking and gating (Q50R, A103V, E105A, D132H, and D132N). Arrhythmia observed in carriers of these CaM variants likely do not arise from direct effect on baseline I_{Ks} or KCNQ1 current.

Clinically, β -blockers are commonly used as medical therapy to treat calmodulinopathy. Still, β -blockers are not equally efficacious in all patients, with more than half of medically treated patients experiencing breakthrough events including sudden cardiac death (17). Risk stratification for patients most likely to benefit from β -blockade would allow for better therapeutic outcomes. Given the key role of KCNQ1 in the fight-or-flight response, CaM variants that perturb KCNQ1 function (e.g. CaM E141G and Q136P) are more likely to derive therapeutic benefits from

β -adrenergic blockade. This study therefore provides data that may inform personalized medical therapy (e.g. β -blocker) in CaM variant carriers.

CaM variant interaction with KCNQ1 in relation to other CaM targets

In this study, several CaM variants do not alter baseline KCNQ1 gating or membrane trafficking, despite binding KCNQ1 with WT-like affinity. Although these variants likely do not impact the cardiac action potential by directly modulating KCNQ1 current, KCNQ1 may still play a role by altering the variant interaction with other CaM regulatory targets. The pool of free CaM in cardiomyocytes has been estimated to be severely limited at 50–75 nM (61). The low supply of free CaM may lead to redistribution of CaM variants on distinct CaM targets depending on relative affinities. For example, KCNQ1 may act as a protective “sink” by sequestering CaM variants that bind KCNQ1 with high affinity without affecting I_{Ks} current, effectively chelating these variants from affecting alternate targets.

Taken together, our study furnishes extensive characterization of CaM variant interaction and effect on KCNQ1 channels, delineating the CaM variants that cause KCNQ1 dysfunction to play a role in arrhythmogenesis. This study demonstrates that KCNQ1 dysfunction is a critical consideration of CaM-induced arrhythmia. The multipronged approach employed in this study of measuring binding, surface expression, and channel function can be readily applied to other CaM binding targets. In all, our findings provide key results toward elucidating calmodulinopathy mechanism that integrates numerous CaM regulatory targets.

Materials and methods

Molecular biology, cell culture, and transfection

Point mutations were made in KCNQ1 channel and CaM utilizing overlap extension and high-fidelity PCR. DNA sequencing confirmed the presence of all mutants made in the final DNA products. For FRET experiments, CHO cells were cultured in 35 mm dishes and transfected with jetPRIME or jetOPTIMUS reagents (Polyplus-transfection, New York, NY) with 4:2 DNA mass ratio for KCNQ1:CaM corresponding to 0.4:0.2 μ g of DNA.

Electrophysiology and FRET solutions

For all solutions, concentrations are in milli-molar (mM) unless otherwise indicated.

Electrophysiology solutions

ND96 solution: NaCl 96, KCl 2, $CaCl_2$ 1.8, $MgCl_2$ 1, HEPES 5, Na pyruvate 2.5, penicillin–streptomycin 100 U/mL. pH adjusted to 7.6 with NaOH. OR2 solution: NaCl 82.5, KCl 2.5, $MgCl_2$ 1, HEPES 5. pH to 7.6 with NaOH.

FRET solutions

HBSS (calcium, magnesium, no phenol red): $CaCl_2$ 1.26, $MgCl_2$ 0.49, $MgSO_4$ 0.41, KCl 5.33, KH_2PO_4 0.44, $NaHCO_3$ 4.17, NaCl 137.93, Na_2HPO_4 0.34, D-glucose 5.56. HBSS was purchased from Thermo Fisher Scientific (Waltham, MA). High Ca^{2+} ($10Ca^{2+}$) solution: NaCl 138, KCl 4, $MgCl_2$ 1, $CaCl_2$ 10, $NaHPO_4$ 0.2, HEPES 10, D-glucose 5. pH to 7.4 with NaOH.

FRET imaging

For all FRET experiments, same-batch transfection of appropriate donor only (e.g. Cerulean-tagged CaM), acceptor only (e.g.

Venus-tagged KCNQ1), and spurious FRET constructs (e.g. Venus-tagged KCNQ1 and untagged Cerulean) were also performed and imaged. When FRET data between mutant constructs were collected (e.g. Venus-tagged KCNQ1 and Cerulean-tagged CaM-mutant), the WT FRET pair was also transfected for same-day comparison. Prior to imaging, each plate was washed three times with PBS solution and incubated in HBSS(+/+) solution (Thermo Fisher Scientific, Waltham MA) at 37°C for imaging. For experiments involving elevating intracellular Ca²⁺, cells were washed and incubated in 10Ca²⁺ solution with freshly mixed 4 μM ionomycin for at least 15 min prior to imaging.

FRET data collection was performed on a Nikon Eclipse Ti-U inverted microscope. Our system design functioned analogously to the “3-cube” FRET technique in which three fluorescence channels were acquired (47, 64), but we implemented multiple bandpass filters, optical splitter, and electronically triggered light source and camera to acquire the three channels without using multiple filter cubes. For the Cerulean–Venus or cyan fluorescent protein (CFP)–yellow fluorescent protein (YFP) FRET pair, cells were excited with the Spectra III light engine (Lumencor, Beaverton, OR) coupled to the microscope through a liquid light guide with the CFP (integrated bandpass filter: 440/20 nm) and YFP (integrated bandpass filter: 510/25 nm) lines. The microscope was outfitted with a triple-band dichroic beamsplitter (FF459/526/596-Di01, Semrock, Rochester, NY) and a triple-band emitter (FF01-475/543/702-25, Semrock, Rochester, NY). The microscope’s filter cube allowed both CFP and YFP lines from Spectra III to excite the cells and simultaneously collected fluorescence emission output from both CFP and YFP at 475 and 543 nm. The fluorescence output was passed into an OptoSplit II Bypass emission image splitter (Cairn Research, Faversham, UK) fitted with a 505 nm beamsplitter (T505lpxr, Chroma Color Corporation, McHenry, IL), 480 nm emission filter (ET480/40 m, Chroma Color Corporation, McHenry, IL), and 545 nm emission filter (ET545/40 m, Chroma Color Corporation, McHenry, IL). The OptoSplit II Bypass effectively separated the fluorescence output into distinct CFP and YFP emission bands. The two bands were directed toward an Andor iXon EMCCD camera (Andor Technology, Belfast, UK) with each band utilizing one-half of the camera sensor for signal detection driven by the Andor Solis software (Andor Technology, Belfast, UK). The two halves of the camera sensor therefore captured both the CFP and YFP emissions simultaneously. The Spectra III light engine and the Andor iXon EMCCD camera were connected to a Digidata 1440A low-noise data acquisition system (Molecular Devices, San Jose, CA) that synchronized both devices by TTL. The Digidata was driven by pClamp software (Molecular Devices, San Jose, CA).

During FRET imaging, the camera was used to locate fluorescence cells for imaging through a 20× objective (Nikon CFI S Plan Fluor 20×/0.45). Once an appropriate field of view was found, the Digidata electronically triggered the Spectra III to turn on the CFP and the YFP lines one after the other, during which the Digidata also triggered the camera to acquire two images. The first image corresponded to excitation by the CFP line only, while the second image corresponded to excitation by the YFP line only. As the Optosplit II ensured the camera simultaneously captured CFP and YFP emission, our protocol enabled collection of three fluorescence channels: (i) CFP excitation and CFP emission (donor channel), (ii) CFP excitation and YFP emission (FRET channel), and (iii) YFP excitation and YFP emission (acceptor channel).

After FRET image acquisition, the images were analyzed and binding curves fitted between KCNQ1 and CaM with MATLAB as detailed in [Extended Methods](#) and in prior studies (47, 52).

Xenopus oocytes harvesting and TEVC

Xenopus laevis (frogs) were housed in the professional animal facility within the Washington University Danforth campus and oocytes harvested from adult female by laparotomy. All procedures were approved by the Washington University Institutional Animal Care and Use Committee Office. Each oocyte was injected with 10–20 ng of cRNA encoding for KCNQ1, KCNE1, or CaM with a Drummond Nanoject (Broomall, PA). For experiments involving multiple constructs, the cRNA were coinjected at 3:1 (KCNQ1:KCNE1), 1:1 (KCNQ1:CaM), and 3:1:4 (KCNQ1:KCNE1:CaM) mass ratio. Injected oocytes were individually incubated in ND96 in 48-well plates at 18°C for 2 to 6 days prior to TEVC recording.

KCNQ1 membrane trafficking efficiency assay

The trafficking efficiency assay experiments were performed with a Zeiss LSM 880 Airyscan two-photon confocal microscope located within the Washington University Center for Cellular Imaging (WUCCI) on the Washington University Medical School campus. CHO cells were transfected in a similar manner to samples prepared for FRET imaging. The cells were plated on 35-mm plates with a small glass-bottom section used for oil immersion imaging. CHO cells were cotransfected with the CaM variant of interest and KCNQ1-psWT-HA-Cer (Fig. 3A). In each experiment, the Alexa-594 were conjugated to the plasma membrane-bound KCNQ1 via a secondary antibody targeted to the HA tag within the S1-S2 linker. During staining, cells were fixed but not permeabilized through PFA fixation to minimize intracellular labeling. To prevent nonspecific labeling of Alexa-594, cells were incubated overnight with BSA at 4°C after fixation. As all KCNQ1 subunits are labeled with a Cerulean probe, the fluorescence intensity in the Cerulean channel is proportional to the total number of KCNQ1 in each cell. On the other hand, the fluorescence intensity of the Alexa-594 channel is proportional to the number of plasma membrane-bound KCNQ1, as the HA tag labeling site is within the extracellular S1-S2 linker. The apparent trafficking efficiency of KCNQ1 was computed for each cell with the equation

$$\text{Apparent trafficking efficiency} = (I_{\text{Alex-594}}) / (I_{\text{Cerulean}})$$

where $I_{\text{Alex-594}}$ and I_{Cerulean} are the fluorescence intensities of the Alexa-594 and Cerulean channels, respectively. All measurements were taken at the same PMT and laser intensity levels. Statistical results are ANOVA tests compared with the WT CaM trafficking efficiency.

Electrophysiology data analysis

Data analysis was performed with MATLAB (MathWorks, MA). G–V curves were quantified by fitting a single Boltzmann function. The instantaneous tail currents following test pulses were normalized to the maximum tail current and fitted with the equation

$$G(V) = (1 + \exp(-V_S \cdot [V - V_{1/2}]))^{-1}$$

where V is the test voltage, V_S is the slope factor controlling the steepness of the Boltzmann equation, and $V_{1/2}$ is the half-activation voltage. V_S is further related to RT/zF , where R is the gas constant, T is the absolute temperature, z is the equivalent valence, and F is the Faraday constant.

KCNQ1 current activation kinetics were quantified by fitting the 4 s test pulse currents with a biexponential function in the general form of

$$I(t) = A_{\text{fast}} \left(1 - \exp\left(-\frac{t - t_{\text{lag}}}{\tau_{\text{fast}}}\right) \right) + A_{\text{slow}} \left(1 - \exp\left(-\frac{t - t_{\text{lag}}}{\tau_{\text{slow}}}\right) \right) + C_{\text{offset}}$$

with one fast component and one slow component. Each exponential is characterized by a time constant τ as well as a steady-state amplitude A . The variable t_{lag} corresponds to the time lag to begin kinetics fitting. Current data between the start of the test pulse and t_{lag} (i.e. $I(0 < t < t_{\text{lag}})$) were not included in the fit. Kinetics fitting of I_{Ks} current activation used a similar equation, but only a single exponential component was used.

For fitting, each current trace was baseline corrected with the mean current at the holding potential (-80 mV) for each trace. With KCNQ1 specifically, as the slow component contained more data points than the fast component, the fast current component was first estimated by fitting the first 0.5 s after the test pulse. A second overall fit was then applied to the entire 4 s test pulse current, with the fast time constant constrained to $\pm 25\%$ of the first fit. For KCNQ1 current activation kinetics, the fraction of the total current carried by the fast component was calculated with the following equation:

$$f_{\text{fast}} = \frac{A_{\text{fast}}}{A_{\text{fast}} + A_{\text{slow}}}$$

Because KCNQ1 current activates without very significant lag, t_{lag} variable was set to zero. On the other hand, t_{lag} was a free parameter in I_{Ks} kinetics fitting. t_{lag} was determined automatically by linear extrapolation. First, the derivative of the current trace was estimated and smoothed by the “diff” and “smooth” functions on MATLAB, respectively. The value of the maximum rate of change ($m_{\text{rate,max}}$) and the time point at which maximum rate of change occurred ($t_{\text{rate,max}}$) within the first 0.4 s was then determined. Using these two parameters, a tangent line was drawn on the current trace at $t = t_{\text{rate,max}}$ with slope $m_{\text{rate,max}}$. Finally, t_{lag} was determined by linear extrapolating the tangent line back to the time point where the line intersects with the instantaneous current at beginning of the test pulse using the equation

$$t_{\text{lag}} = t_{\text{rate,max}} - \left(\frac{I(t = t_{\text{rate,max}}) - I(t = 0)}{m_{\text{rate,max}}} \right)$$

Supplementary Material

Supplementary material is available at PNAS Nexus online.

Funding

This work was supported by grants National Institutes of Health (NIH) R01 HL136553 and R01 NS092570 (J.R.S.), NIH R01 HL155398 (J.C.), NIH F30 HL151042 (P.w.K.), and US–Israel Binational Science Foundation research grant 2019159 (J.C.).

Author Contributions

P.w.K., J.C., and J.R.S. conceptualized and designed the research; P.w.K., L.W., P.A., J.S., M.M., C.A., D.Z., N.S., and A.B. performed the research and acquired data, P.w.K., L.W., and N.S. analyzed

the data; J.R.S. and J.C. acquired funding; P.w.K. and L.W. made figures and wrote the original draft, and all authors revised the manuscript.

Preprints

This manuscript was posted on a preprint: <https://doi.org/10.1101/2023.01.28.526031>.

Data Availability

All data required to evaluate the conclusions within this manuscript are presented in the main text and the supplements.

References

- Ben-Johny M, Yue DT. 2014. Calmodulin regulation (calmodulation) of voltage-gated calcium channels. *J gen Physiol.* 143(6): 679–692.
- Meissner G. 2017. The structural basis of ryanodine receptor ion channel function. *J Gen Physiol.* 149(12):1065–1089.
- Sorensen AB, Søndergaard MT, Overgaard MT. 2013. Calmodulin in a heartbeat. *FEBS J.* 280(21):5511–5532.
- Van Petegem F. 2012. Ryanodine receptors: structure and function. *J Biol Chem.* 287(38):31624–31632.
- Shamgar L, et al. 2006. Calmodulin is essential for cardiac IKs channel gating and assembly: impaired function in long-QT mutations. *Circ Res.* 98(8):1055–1063.
- Ghosh S, Nunziato DA, Pitt GS. 2006. KCNQ1 assembly and function is blocked by long-QT syndrome mutations that disrupt interaction with calmodulin. *Circ Res.* 98(8):1048–1054.
- Ben-Johny M, et al. 2014. Conservation of Ca₂+calmodulin regulation across Na and Ca₂+ channels. *Cell* 157(7):1657–1670.
- Adams PJ, Ben-Johny M, Dick IE, Inoue T, Yue DT. 2014. Apocalmodulin itself promotes ion channel opening and Ca(2+) regulation. *Cell* 159(3):608–622.
- Kang PW, et al. 2021. Elementary mechanisms of calmodulin regulation of Na(V)1.5 producing divergent arrhythmogenic phenotypes. *Proc Natl Acad Sci U S A.* 118:21.
- Kang PW, et al. 2020. Calmodulin acts as a state-dependent switch to control a cardiac potassium channel opening. *Sci Adv.* 6:50.
- Yan H, Wang C, Marx SO, Pitt GS. 2017. Calmodulin limits pathogenic Na+ channel persistent current. *J Gen Physiol.* 149(2): 277–293.
- Urrutia J, et al. 2019. The crossroad of ion channels and calmodulin in disease. *Int J Mol Sci.* 20:400.
- Bauer R, Timothy KW, Golden A. 2021. Update on the molecular genetics of Timothy syndrome. *Front Pediatr.* 9:668546.
- Hussey JW, Limpitikul WB, Dick IE. 2023. Calmodulin mutations in human disease. *Channels (Austin).* 17(1):2165278.
- Friedberg F, Rhoads AR. 2001. Evolutionary aspects of calmodulin. *IUBMB Life.* 51(4):215–221.
- Crotti L, et al. 2013. Calmodulin mutations associated with recurrent cardiac arrest in infants. *Circulation* 127(9):1009–1017.
- Crotti L, et al. 2019. Calmodulin mutations and life-threatening cardiac arrhythmias: insights from the International Calmodulinopathy Registry. *Eur Heart J.* 40(35):2964–2975.
- Nyegaard M, et al. 2012. Mutations in calmodulin cause ventricular tachycardia and sudden cardiac death. *Am J Hum Genet.* 91(4): 703–712.
- Jensen HH, Brohus M, Nyegaard M, Overgaard MT. 2018. Human calmodulin mutations. *Front Mol Neurosci.* 11:396.

- 20 Chazin WJ, Johnson CN. 2020. Calmodulin mutations associated with heart arrhythmia: a status report. *Int J Mol Sci.* 21:1418.
- 21 Makita N, et al. 2014. Novel calmodulin mutations associated with congenital arrhythmia susceptibility. *Circ Cardiovasc Genet.* 7(4):466–474.
- 22 Boczek NJ, et al. 2016. Spectrum and prevalence of CALM1-, CALM2-, and CALM3-encoded calmodulin variants in long QT syndrome and functional characterization of a novel long QT syndrome-associated calmodulin missense variant, E141G. *Circ Cardiovasc Genet.* 9(2):136–146.
- 23 Søndergaard MT, et al. 2017. The arrhythmogenic calmodulin p.Phe142Leu mutation impairs C-domain Ca²⁺ binding but not calmodulin-dependent inhibition of the cardiac ryanodine receptor. *J Biol Chem.* 292(4):1385–1395.
- 24 Søndergaard MT, et al. 2015. Calmodulin mutations causing catecholaminergic polymorphic ventricular tachycardia confer opposing functional and biophysical molecular changes. *FEBS J.* 282(4):803–816.
- 25 Wren LM, et al. 2019. Genetic mosaicism in calmodulinopathy. *Circ Genom Precis Med.* 12(9):375–385.
- 26 Hwang HS, et al. 2014. Divergent regulation of ryanodine receptor 2 calcium release channels by arrhythmogenic human calmodulin missense mutants. *Circ Res.* 114(7):1114–1124.
- 27 Brohus M, et al. 2021. Infanticide vs. inherited cardiac arrhythmias. *Europace.* 23(3):441–450.
- 28 Kato K, et al. 2022. Novel CALM3 variant causing calmodulinopathy with variable expressivity in a 4-generation family. *Circ Arrhythmia Electrophysiol.* 15(3):e010572.
- 29 Limpitikul WB, et al. 2014. Calmodulin mutations associated with long QT syndrome prevent inactivation of cardiac L-type Ca²⁺ currents and promote proarrhythmic behavior in ventricular myocytes. *J Mol Cell Cardiol.* 74:115–124.
- 30 Limpitikul WB, et al. 2017. A precision medicine approach to the rescue of function on malignant calmodulinopathic long-QT syndrome. *Circ Res.* 120(1):39–48.
- 31 Yin G, et al. 2014. Arrhythmogenic calmodulin mutations disrupt intracellular cardiomyocyte Ca²⁺ regulation by distinct mechanisms. *J Am Heart Assoc.* 3(3):e000996.
- 32 Wang K, et al. 2020. Arrhythmia mutations in calmodulin can disrupt cooperativity of Ca²⁺ binding and cause misfolding. *J Physiol.* 598(6):1169–1186.
- 33 Wang K, et al. 2018. Arrhythmia mutations in calmodulin cause conformational changes that affect interactions with the cardiac voltage-gated calcium channel. *Proc Natl Acad Sci U S A.* 115(45):E10556–e10565.
- 34 Rocchetti M, et al. 2017. Elucidating arrhythmogenic mechanisms of long-QT syndrome CALM1-F142L mutation in patient-specific induced pluripotent stem cell-derived cardiomyocytes. *Cardiovasc Res.* 113(5):531–541.
- 35 Sun J, MacKinnon R. 2017. Cryo-EM structure of a KCNQ1/CaM complex reveals insights into congenital long QT syndrome. *Cell.* 169(6):1042–1050.e9.
- 36 Sanguinetti MC, et al. 1996. Coassembly of K(V)LQT1 and minK (IsK) proteins to form cardiac I(Ks) potassium channel. *Nature.* 384(6604):80–83.
- 37 Barhanin J, et al. 1996. K(V)LQT1 and IsK (minK) proteins associate to form the I(Ks) cardiac potassium current. *Nature.* 384(6604):78–80.
- 38 Sun J, MacKinnon R. 2019. Structural basis of human KCNQ1 modulation and gating. *Cell.* 180(2):340–347.e9.
- 39 Sachyani D, et al. 2014. Structural basis of a Kv7.1 potassium channel gating module: studies of the intracellular c-terminal domain in complex with calmodulin. *Structure.* 22(11):1582–1594.
- 40 Bartos DC, Morotti S, Ginsburg KS, Grandi E, Bers DM. 2017. Quantitative analysis of the Ca²⁺-dependent regulation of delayed rectifier K⁺ current IKs in rabbit ventricular myocytes. *J Physiol.* 595(7):2253–2268.
- 41 Tobelaim WS, et al. 2017. Competition of calcified calmodulin N lobe and PIP2 to an LQT mutation site in Kv7.1 channel. *Proc Natl Acad Sci U S A.* 114(5):E869–E878.
- 42 Hou P, et al. 2020. Two-stage electro-mechanical coupling of a KV channel in voltage-dependent activation. *Nat Commun.* 11(1):676.
- 43 Taylor KC, et al. 2020. Structure and physiological function of the human KCNQ1 channel voltage sensor intermediate state. *eLife.* 9:e53901.
- 44 Zaydman MA, et al. 2014. Domain-domain interactions determine the gating, permeation, pharmacology, and subunit modulation of the IKs ion channel. *eLife.* 3:e03606.
- 45 Erickson MG, Liang H, Mori MX, Yue DT. 2003. FRET two-hybrid mapping reveals function and location of L-type Ca²⁺ channel CaM preassociation. *Neuron.* 39(1):97–107.
- 46 Bal M, Zaika O, Martin P, Shapiro MS. 2008. Calmodulin binding to M-type K⁺ channels assayed by TIRF/FRET in living cells. *J Physiol.* 586(9):2307–2320.
- 47 Rivas S, Hanif K, Chakouri N, Ben-Johny M. 2021. Probing ion channel macromolecular interactions using fluorescence resonance energy transfer. *Methods Enzymol.* 653:319–347.
- 48 Alberdi A, et al. 2015. Uncoupling PIP2-calmodulin regulation of Kv7.2 channels by an assembly destabilizing epileptogenic mutation. *J Cell Sci.* 128(21):4014–4023.
- 49 Koushik SV, Chen H, Thaler C, Puhl HL 3rd, Vogel SS (2006) Cerulean, Venus, and VenusY67C FRET reference standards. *Biophys J.* 91(12):L99–L101.
- 50 Haitin Y, et al. 2009. Intracellular domains interactions and gated motions of I(KS) potassium channel subunits. *EMBO J.* 28(14):1994–2005.
- 51 Ben-Johny M, Yue DN, Yue DT. 2016. Detecting stoichiometry of macromolecular complexes in live cells using FRET. *Nat Commun.* 7:13709.
- 52 Butz ES, et al. 2016. Quantifying macromolecular interactions in living cells using FRET two-hybrid assays. *Nat Protoc.* 11(12):2470–2498.
- 53 White DS, et al. 2021. cAMP binding to closed pacemaker ion channels is non-cooperative. *Nature.* 595(7868):606–610.
- 54 Lek M, et al. 2016. Analysis of protein-coding genetic variation in 60,706 humans. *Nature.* 536(7616):285–291.
- 55 Hou P, et al. 2017. Inactivation of KCNQ1 potassium channels reveals dynamic coupling between voltage sensing and pore opening. *Nat Commun.* 8(1):1730.
- 56 Wang Q, et al. 1996. Positional cloning of a novel potassium channel gene: KVLQT1 mutations cause cardiac arrhythmias. *Nat Genet.* 12(1):17–23.
- 57 Cui J, Kline RP, Pennefather P, Cohen IS. 1994. Gating of IsK expressed in *Xenopus* oocytes depends on the amount of mRNA injected. *J Gen Physiol.* 104(1):87–105.
- 58 Pipilas DC, et al. 2016. Novel calmodulin mutations associated with congenital long QT syndrome affect calcium current in human cardiomyocytes. *Heart Rhythm.* 13(10):2012–2019.
- 59 Chang A, et al. 2018. A calmodulin C-lobe Ca²⁺-dependent switch governs Kv7 channel function. *Neuron.* 97(4):836–852.e6.
- 60 Brohus M, Busuioac A-O, Wimmer R, Nyegaard M, Overgaard MT. 2023. Calmodulin mutations affecting Gly114 impair binding to the NaV1.5 IQ-domain. *Front Pharmacol.* 14:1210140.

- 61 Wu X, Bers DM. 2007. Free and bound intracellular calmodulin measurements in cardiac myocytes. *Cell Calcium* 41(4):353–364.
- 62 Bogdanov V, et al. 2022. Spatially and functionally distinct pools of calmodulin mRNA in cardiac myocytes. *Biophys J.* 121(3, Supplement 1):257a.
- 63 Kim CW, Aronow WS, Dutta T, Frenkel D, Frishman WH. 2020. Catecholaminergic polymorphic ventricular tachycardia. *Cardiol Rev.* 28(6):325–331.
- 64 Erickson MG, Alseikhan BA, Peterson BZ, Yue DT. 2001. Preassociation of calmodulin with voltage-gated Ca(2+) channels revealed by FRET in single living cells. *Neuron* 31(6):973–985.